

1  
2  
3  
4  
5  
6  
7  
8  
9  
10  
11  
12  
13  
14  
15  
16  
17  
18  
19  
20  
21  
22  
23  
24  
25  
26  
27  
28  
29  
30  
31  
32  
33  
34  
35  
36  
37  
38

**A robust Upwind Mixed Hybrid Finite Element method for transport  
in variably saturated porous media**

Anis Younes<sup>1\*</sup>, Hussein Hoteit<sup>2</sup>, Rainer Helmig<sup>3</sup>, Marwan Fahs<sup>1</sup>

<sup>1</sup>Institut Terre et Environnement de Strasbourg, Université de Strasbourg, CNRS, ENGEES, UMR 7063, 67084  
Strasbourg, France

<sup>2</sup>Physical Science and Engineering Division, King Abdullah University of Science and Technology (KAUST),  
Thuwal, Saudi Arabia

<sup>3</sup> Institute for Modelling Hydraulic and Environmental Systems, University of Stuttgart, Pfaffenwaldring 61,  
70569 Stuttgart, Germany

*Submitted to Hydrology and Earth System Sciences (HESS)*

Contact author: Anis Younes

E-mail: [younes@unistra.fr](mailto:younes@unistra.fr)

39 **Abstract**

40 The Mixed Finite Element (MFE) method is well adapted for the simulation of fluid flow in  
41 heterogeneous porous media. However, when employed for the transport equation, it can  
42 generate solutions with strong unphysical oscillations because of the hyperbolic nature of  
43 advection. In this work, a robust upwind MFE scheme is proposed to avoid such unphysical  
44 oscillations. The new scheme is a combination of the upwind edge/face centred finite volume  
45 method with the hybrid formulation of the MFE method. The scheme ensures continuity of  
46 both advective and dispersive fluxes between adjacent elements and allows to maintain the  
47 time derivative continuous, which permits employment of high order time integration  
48 methods via the Method of Lines (MOL).

49 Numerical simulations are performed in both saturated and unsaturated porous media to  
50 investigate the robustness of the new upwind-MFE scheme. Results show that, contrarily to  
51 the standard scheme, the upwind-MFE method generates stable solutions without under and  
52 overshoots. The simulation of contaminant transport into a variably saturated porous medium  
53 highlights the robustness of the proposed upwind scheme when combined with the MOL for  
54 solving nonlinear problems.

55

56 ***Keywords:***

57 Hybrid Mixed Finite Element, upwind scheme, advection-dispersion transport, numerical  
58 oscillations, Method of Lines.

59

60

## 61 **1. Introduction**

62 The Mixed Finite Element (MFE) method (Raviart and Thomas, 1977; Brezzi *et al.*, 1985;  
63 Chavent and Jaffré, 1986; Brezzi and Fortin, 1991, Younes *et al.*, 2010) is known to be a  
64 robust numerical scheme for solving elliptic diffusion problems such as the fluid flow in  
65 heterogeneous porous media. The method combines advantages of the finite volumes, by  
66 ensuring local mass conservation and continuity of fluxes between adjacent cells, and  
67 advantages of finite elements by easily handling heterogeneous domains with discontinuous  
68 parameter distributions and unstructured meshes. As a consequence, the MFE method has  
69 been largely used for flow in porous media (see, for instance, the review of Younes *et al.*  
70 (2010) and references therein). The hybridization technique has been largely used with the  
71 MFE method to improve its efficiency (Chavent and Roberts, 1991; Traverso *et al.* 2013).  
72 This technique allows to reduce the total number of unknowns and produces a final system  
73 with a symmetric positive definite matrix. The unknowns with the hybrid-MFE method are  
74 the Lagrange multipliers which correspond to the traces of the scalar variable at edges/faces  
75 (Chavent and Jaffré, 1986).

76 When applied to transient diffusion equations with small time steps, the hybrid-MFE method  
77 can produce solutions with small unphysical over and undershoots (Hoteit *et al.*, 2002a,  
78 2002b; Mazzia, 2008). A lumped formulation of the hybrid-MFE method was developed by  
79 Younes *et al.* (2006) to improve its monotonicity and reduce nonphysical oscillations. The  
80 lumped formulation ensures that the maximum principle is respected for parabolic diffusion  
81 equations on acute triangulations (Younes *et al.*, 2006). For more general 2D and 3D element  
82 shapes, the lumping procedure allows to significantly improve the monotonous character of  
83 the hybrid-MFE solution (Younes *et al.*, 2006; Koohbor *et al.*, 2020). As an illustration, the  
84 lumped formulation was shown to be more efficient and more robust than the standard hybrid  
85 formulation for the simulation of the challenging nonlinear problem of water infiltration into

86 an initially dry soil (Belfort *et al.*, 2009). The lumped formulation has recently been used for  
87 flow discretization in the case of density driven flow in saturated-unsaturated porous media  
88 (Younes *et al.*, 2022a).

89 However, the MFE method remains little used for the discretization of the full transport  
90 equation. When employed to the advection-dispersion equation, the MFE method can  
91 generate solutions with strong numerical instabilities in the case of advection-dominated  
92 transport because of the hyperbolic nature of the advection operator. To avoid these  
93 instabilities, one of the most popular and easiest ways is to use an upwind scheme. Indeed,  
94 although upwind schemes introduce some numerical diffusion leading to an artificial  
95 smearing of the numerical solution, they avoid unphysical oscillations and remain useful,  
96 especially for large domains and regional field simulations. In the literature, some upwind  
97 mixed finite element schemes have been employed to improve the robustness of the MFE  
98 method for advection-dominated problems (Dawson, 1998; Dawson and Aizinger, 1999;  
99 Radu *et al.*, 2011; Vohralik, 2007; Brunner *et al.*, 2014).

100 The main idea of an upwind scheme for an element  $E$ , is to calculate the mass flux exchanged  
101 with its adjacent element  $E'$  using the concentration from  $E$  in the case of an outflow and the  
102 concentration from  $E'$  in the case of an inflow. However, this idea cannot be applied as such  
103 with the hybrid-MFE method since the hybridization procedure requires to express the flux at  
104 the element interface as only a function of variables at the element  $E$  (and not  $E'$ ). To  
105 overcome this difficulty, Radu *et al.* (2011), and Brunner *et al.* (2014) proposed an upwind  
106 MFE method where, in the case of an inflow, the concentration at the adjacent element  $E'$  is  
107 replaced by an approximation using the concentration at  $E$  and the trace of concentration at  
108 the interface  $\partial_{EE'}$  by assuming that the edge concentration is the mean of the concentrations in  
109  $E$  and  $E'$ . However, this assumption cannot be verified for a general configuration.

110 Furthermore, with such an assumption, each of the advective and dispersive fluxes is  
111 discontinuous at the element interfaces, and continuity is only fulfilled for the total flux.

112 In this work, a new upwind-MFE method is proposed for solving the full transport equation  
113 without requiring any approximation of the upwind concentration. The new scheme is a  
114 combination of the upwind edge/face centered finite volume (FV) scheme with the lumped  
115 formulation of the MFE method. It guarantees continuity of both advective and dispersive  
116 fluxes at element interfaces. Further, the new upwind-MFE scheme maintains the time  
117 derivative continuous and thus, allows to employ high order time integration methods via the  
118 method of lines (MOL), which was shown to be very efficient for solving nonlinear problems  
119 (see, for instance, Fahs *et al.* (2009) and Younes *et al.* (2009)).

120 This article is structured as follows. In section 2, we recall the hybrid-MFE method for the  
121 discretization of the transport equation. In section 3, we introduce the new upwind-MFE  
122 method based on the combination of the upwind edge/face FV scheme with the lumped  
123 formulation of the MFE method. In section 4, numerical experiments are performed for  
124 transport in saturated and unsaturated porous media to investigate the robustness of the new  
125 developed upwind-MFE scheme. Some conclusions are given in the last section of the article.

## 126 **2. The hybrid-MFE method for the advection-dispersion equation**

127 The mass conservation of the contaminant in variably saturated porous media is:

$$128 \quad \frac{\partial(\theta C)}{\partial t} + \nabla \cdot (\tilde{\mathbf{q}}_a + \tilde{\mathbf{q}}_d) = 0 \quad (1)$$

129 where  $C$  is the normalized concentration [-],  $\theta$  is water content [ $L^3L^{-3}$ ],  $t$  is time [T],

130  $\tilde{\mathbf{q}}_a = \mathbf{q}C$  is the advective flux with  $\mathbf{q}$  the Darcy velocity [ $LT^{-1}$ ] and  $\tilde{\mathbf{q}}_d$  the dispersive flux

131 given by:

$$132 \quad \tilde{\mathbf{q}}_d = -\mathbf{D}\nabla C \quad (2)$$

133 with  $\mathbf{D}$ , the dispersion tensor, expressed by:

134 
$$\mathbf{D} = D_m \mathbf{I} + (\alpha_L - \alpha_T) \mathbf{q} \otimes \mathbf{q} / |\mathbf{q}| + \alpha_T |\mathbf{q}| \mathbf{I} \quad (3)$$

135 in which  $\alpha_L$  and  $\alpha_T$  are the longitudinal and transverse dispersivities [L],  $D_m$  is the pore  
 136 water diffusion coefficient [ $L^2T^{-1}$ ] and  $\mathbf{I}$  is the unit tensor.

137 The water content  $\theta$  and the Darcy velocity  $\mathbf{q}$  are linked by the fluid mass conservation  
 138 equation in variably saturated porous media:

139 
$$\frac{\partial \theta}{\partial t} + \nabla \cdot \mathbf{q} = 0 \quad (4)$$

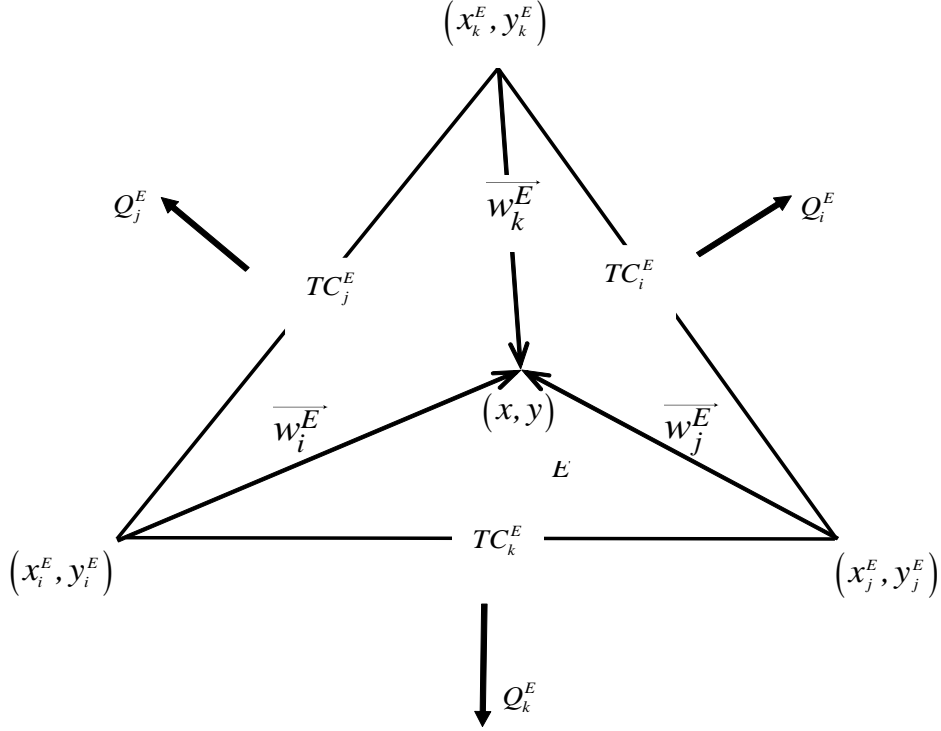
140 Substituting Eq. (4) into Eq. (1) yields the following advection-dispersion equation:

141 
$$\theta \frac{\partial C}{\partial t} + \nabla \cdot (\tilde{\mathbf{q}}_a + \tilde{\mathbf{q}}_d) - C \nabla \cdot \mathbf{q} = 0 \quad (5)$$

142 In this work, we consider that the velocity  $\mathbf{q}$  is obtained by solving Richards' equation using  
 143 the hybrid-MFE method. For a two-dimensional domain with a triangular mesh,  $\mathbf{q}$  is  
 144 approximated inside each triangle  $E$  using the lowest-order Raviart-Thomas (RT0) vectorial  
 145 basis functions  $\mathbf{w}_j^E$ :

146 
$$\mathbf{q} = \sum_{j=1}^3 Q_j^E \mathbf{w}_j^E \quad (6)$$

147 where  $Q_j^E$  is the water flux across the edge  $E_j$  of  $E$  (see Figure 1) and  $\mathbf{w}_j^E = \frac{1}{2|E|} \begin{pmatrix} x - x_j^E \\ y - y_j^E \end{pmatrix}$   
 148 is the typical RT0 basis functions (Younes *et al.*, 1999) with  $(x_j^E, y_j^E)$  the coordinates of the  
 149 node  $j$  opposite to the edge  $E_j$  of  $E$  and  $|E|$ , the area of  $E$ .



150

151

Figure 1: Vectorial basis functions for the MFE method.

152

153 To apply the hybrid-MFE method to the transport Eq. (5), we approximate the dispersive flux

154  $\tilde{\mathbf{q}}_d$  with RT0 vectorial basis functions as:

155 
$$\tilde{\mathbf{q}}_d = \sum_{j=1}^3 \tilde{Q}_j^{d,E} \mathbf{w}_j^E \quad (7)$$

156 where  $\tilde{Q}_j^{d,E} = \int_{E_j} \tilde{\mathbf{q}}_d \cdot \boldsymbol{\eta}_j^E$  is the dispersive flux across the edge  $E_j$  of the element  $E$  and  $\boldsymbol{\eta}_j^E$  is

157 the outward unit normal vector to the edge  $E_j$ .

158 The variational formulation of Eq. (2) using the test function  $\mathbf{w}_i^E$  yields:

159 
$$\int_E \mathbf{D}^{-1} \tilde{\mathbf{q}}_d \cdot \mathbf{w}_i^E = \int_E \mathbf{C} \nabla \cdot \mathbf{w}_i^E - \sum_j \int_{E_j} \mathbf{C} \mathbf{w}_i^E \cdot \boldsymbol{\eta}_j^E \quad (8)$$

160 Substituting Eq. (7) into Eq. (8) and using properties of the basis functions  $\mathbf{w}_j^E$  give

161 
$$\sum_j \tilde{Q}_j^{d,E} \int_E (\mathbf{D}_E^{-1} \mathbf{w}_j^E) \cdot \mathbf{w}_i^E = \frac{1}{|E|} \int_E C - \frac{1}{|E_i|} \int_{E_i} C$$
 (9)  
 162 
$$= C_E - TC_i^E$$

162 in which,  $\mathbf{D}_E$  is the local dispersion tensor at the element  $E$ ,  $C_E$  is the mean concentration at  
 163  $E$  and  $TC_i^E$  is the edge (trace) concentration (Lagrange multiplier) at the edge  $E_i$ .

164 Denoting the local matrix  $\tilde{\mathbf{B}}_{i,j}^E = \int_E (\mathbf{D}_E^{-1} \mathbf{w}_j^E) \cdot \mathbf{w}_i^E$ , the inversion of the system of Eq. (9) gives

165 the expression for the dispersive flux  $\tilde{Q}_i^{d,E}$ :

166 
$$\tilde{Q}_i^{d,E} = \sum_j \tilde{\mathbf{B}}_{i,j}^{E,-1} (C_E - TC_j^E)$$
 (10)

167 Besides, the integration of the mass conservation Eq. (6) over the element  $E$  writes

168 
$$\int_E \theta \frac{\partial C}{\partial t} + \int_E \nabla \cdot \tilde{\mathbf{q}}_a + \int_E \nabla \cdot \tilde{\mathbf{q}}_d - \int_E C \nabla \cdot \mathbf{q} = 0$$
 (11)

169 which becomes, using Green's formula,

170 
$$\theta_E |E| \frac{\partial C_E}{\partial t} + \sum_i \int_{E_i} C \mathbf{q} \cdot \boldsymbol{\eta}_i^E + \sum_i \int_{E_i} \tilde{\mathbf{q}}_d \cdot \boldsymbol{\eta}_i^E - \int_E C \nabla \cdot \mathbf{q} = 0$$
 (12)

171 where  $\theta_E$  is the water content of the element  $E$ .

172 Substituting Eq. (2) into Eq. (12) yields

173 
$$\theta_E |E| \frac{\partial C_E}{\partial t} + \sum_i \underbrace{(\tilde{Q}_i^{a,E} + \tilde{Q}_i^{d,E})}_{\tilde{Q}_i^{t,E}} - C_E \sum_i Q_i^E = 0$$
 (13)

174 in which  $\tilde{Q}_i^{t,E} = \tilde{Q}_i^{a,E} + \tilde{Q}_i^{d,E}$  is the total flux at the edge  $E_i$  with  $\tilde{Q}_i^{a,E}$  the advective flux given

175 by  $\tilde{Q}_i^{a,E} = Q_i^E TC_i^E$  and  $\tilde{Q}_i^{d,E}$  the dispersive flux given by Eq. (10).

176 The hybridization of the MFE method is performed in the following two steps:

177 1) The flux Eq. (10) is substituted into the mass conservation Eq. (13), which is then

178 discretized in time using the first-order implicit Euler scheme



179 
$$\theta_E \frac{|E|}{\Delta t} (C_E^{n+1} - C_E^n) + \sum_i Q_i^E TC_i^{E,n+1} - C_E^{n+1} \sum_i Q_i^E + \tilde{\alpha}^E C_E^{n+1} - \sum_i \tilde{\alpha}_i^E TC_i^{E,n+1} = 0 \quad (14)$$

180 in which  $\tilde{\alpha}_i^E = \sum_j \tilde{B}_{i,j}^{E,-1}$  and  $\tilde{\alpha}^E = \sum_i \tilde{\alpha}_i^E$ .

181 Hence, the mean concentration at the new time level  $C_E^{n+1}$  can be expressed as a function  
 182 of  $TC_i^{E,n+1}$ , the concentration at the edges of  $E$ , as follows:

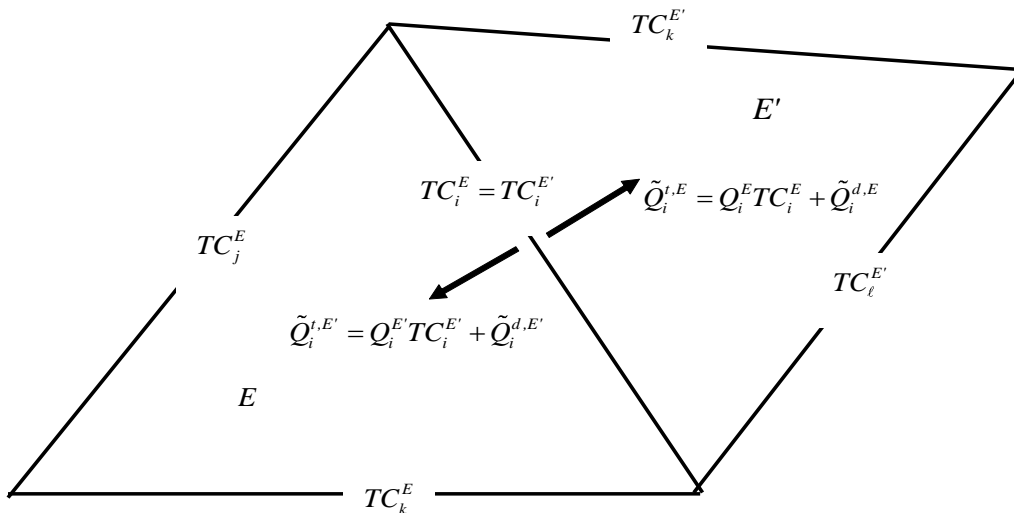
183 
$$C_E^{n+1} = \frac{1}{\beta_E} \sum_i (\tilde{\alpha}_i^E - Q_i^E) TC_i^{E,n+1} + \frac{\lambda_E}{\beta_E} C_E^n \quad (15)$$

184 in which  $\lambda_E = \theta_E \frac{|E|}{\Delta t}$  and  $\beta_E = \left( \lambda_E + \tilde{\alpha}^E - \sum_i Q_i^E \right)$ .

185 The mean concentration given by Eq. (15) is then substituted into the flux Eq. (10), which  
 186 allows expressing the dispersive flux  $\tilde{Q}_i^{d,E,n+1}$  (the subscript n+1 will be omitted to alleviate  
 187 the notations) as only a function of the traces of concentration at edges  $TC_i^{E,n+1}$ :

188 
$$\tilde{Q}_i^{d,E} = \sum_j \left( \frac{\tilde{\alpha}_i^E}{\beta_E} (\tilde{\alpha}_j^E - Q_j^E) - \tilde{B}_{i,j}^{E,-1} \right) TC_j^{E,n+1} + \frac{\lambda_E}{\beta_E} \tilde{\alpha}_i^E C_E^n \quad (16)$$

189 2) The system to be solved is obtained by imposing the continuity of the total flux  
 190 ( $\tilde{Q}_i^{t,E} + \tilde{Q}_i^{t,E'} = 0$ ) as well as the continuity of the trace of concentration ( $TC_i^{E,n+1} = TC_i^{E',n+1}$ )  
 191 at the edge  $i$  between the two elements  $E$  and  $E'$  (Figure 2).



192

193 Figure 2: Continuity of concentration and total flux between adjacent elements with the  
 194 hybrid-MFE method.

195 Note that the advective flux  $\tilde{Q}_i^{a,E}$  is continuous between  $E$  and  $E'$  because of the continuity  
 196 of the water flux and the continuity of the trace of concentration at the interface. Thus, for  
 197 the continuity of the total flux ( $\tilde{Q}_i^{t,E} + \tilde{Q}_i^{t,E'} = 0$ ), it is required that the dispersive flux is  
 198 continuous:

$$199 \quad \tilde{Q}_i^{t,E} + \tilde{Q}_i^{t,E'} = (Q_i^E + Q_i^{E'})TC_i^{E,n+1} + \tilde{Q}_i^{d,E} + \tilde{Q}_i^{d,E'} = \tilde{Q}_i^{d,E} + \tilde{Q}_i^{d,E'} = 0 \quad (17)$$

200 Using Eq. (16), we obtain:

$$201 \quad \sum_j \left( \tilde{B}_{i,j}^{E,-1} - \frac{\tilde{\alpha}_i^E}{\beta_E} (\tilde{\alpha}_j^E - Q_j^E) \right) TC_j^{E,n+1} + \sum_j \left( \tilde{B}_{i,j}^{E',-1} - \frac{\tilde{\alpha}_i^{E'}}{\beta_{E'}} (\tilde{\alpha}_j^{E'} - Q_j^{E'}) \right) TC_j^{E',n+1} \quad (18)$$

$$= \frac{\lambda_E}{\beta_E} \tilde{\alpha}_i^E C_E^n + \frac{\lambda_{E'}}{\beta_{E'}} \tilde{\alpha}_i^{E'} C_{E'}^n$$

202 The continuity Eq. (18) is written for all mesh edges, and the resulting equations form the  
 203 final system to be solved for the traces of concentration at edges  $TC_i^{E,n+1}$  as unknowns.

204 Note that the hybrid-MFE Eqs (18), obtained by approximating the dispersive flux with RT0  
 205 basis functions, is equivalent to the new MFE method proposed in Radu *et al.* (2011).

### 206 3. The upwind and lumped MFE approaches

207 In this section, we recall the main principles of two existing approaches, developed to  
 208 improve the stability of the MFE solution of the transport equation. The first approach is the  
 209 upwind-hybrid MFE scheme of Radu *et al.* (2011), developed for advection dominated  
 210 transport. The second approach is the lumped hybrid-MFE method of Younes *et al.* (2006),  
 211 developed for dispersive transport.

#### 212 3.1 The upwind-hybrid MFE of Radu *et al.* (2011)

213

214 In the case of advection-dominated transport, solving the hybrid-MFE Eq. (18) can yield  
 215 solutions with strong instabilities. A common way to avoid such instabilities is to use an  
 216 upwind scheme for the advective flux. Thus, for an element  $E$ , the advective flux  
 217  $\tilde{Q}_i^{a,E} = Q_i^E TC_i^E$  at the edge  $i$  (common with the element  $E'$ ), has to be calculated using either  
 218 the concentration from  $E$  (if  $Q_i^E > 0$ ) or the concentration from  $E'$  (if  $Q_i^E < 0$ ). Radu *et al.*  
 219 (2011) suggested replacing the advective flux  $\tilde{Q}_i^{a,E} = Q_i^E TC_i^E$  at the interface by:

$$220 \quad \tilde{Q}_i^{a,E} = \begin{cases} Q_i^E C^E & \text{if } Q_i^E > 0 \\ Q_i^E C^{E'} & \text{if } Q_i^E < 0 \end{cases} \quad (19)$$

221 The advective term is now calculated using the upwind mean concentration, which can be that  
 222 of the element  $E$  or of its adjacent element  $E'$ .

223 The advective flux of Eq. (19) is rewritten in the following condensed form

$$224 \quad \tilde{Q}_i^{a,E} = Q_i^E \left( \tau_i^E C^E + (1 - \tau_i^E) C^{E'} \right) \quad (20)$$

225 with  $\tau_i^E = 1$  for an outflow ( $Q_i^E > 0$ ) and  $\tau_i^E = 0$  for an inflow ( $Q_i^E < 0$ ).

226 However, this expression is incompatible with the hybridization procedure. Indeed, if we  
 227 replace, in the Eq. (14), the advective term  $Q_i^E TC_i^E$  by Eq. (20), the latter will contain both  
 228  $C^E$  and  $C^{E'}$ . Thus, the first step of the hybridization procedure cannot allow expressing  
 229  $C_E^{n+1}$  as only a function of  $TC_i^{E,n+1}$  as in the Eq. (15).

230 To avoid this difficulty, Radu *et al.* (2011) suggested replacing,  $C^{E'}$  by the following  
 231 expression:

$$232 \quad C^{E'} \simeq 2TC_i^E - C^E \quad (21)$$

233 This approximation is based on the assumption that  $TC_i^E \simeq (C^E + C^{E'})/2$ .

234 Plugging Eq. (21) into Eq. (20), the advective flux  $\tilde{Q}_i^{a,E}$  depends only on the variables of the  
 235 element  $E$  (mean concentration  $C^E$  and edge concentration  $TC_i^E$ ):

236 
$$\tilde{Q}_i^{a,E} = Q_i^E \left( \tau_i^E C^E - (1 - \tau_i^E) C^E + 2(1 - \tau_i^E) TC_i^E \right) \quad (22)$$

237 Eq. (22) can then be used to replace the advective term  $Q_i^E TC_i^{E,n+1}$  in Eq. (14), and thus the  
 238 hybridization procedure allows to express  $C_E^{n+1}$  as a function of  $TC_i^{E,n+1}$  as in the Eq. (15).  
 239 Then, the expression of  $C_E^{n+1}$  is substituted into the dispersive flux Eq. (10), and the final  
 240 system is obtained by prescribing continuity of the total flux ( $\tilde{Q}_i^{t,E} + \tilde{Q}_i^{t,E'} = 0$ ) at the interface  
 241 between  $E$  and  $E'$ . This scheme was shown to be more efficient (by using a sparser system  
 242 matrix with fewer unknowns) than the non-hybrid upwind mixed method of Dawson (1978).  
 243 The two methods yielded optimal first order convergence in time and space (Brunner *et al.*,  
 244 2014).

245 The assumption given by Eq. (21) can be a rough approximation, especially in the case of a  
 246 heterogeneous domain where dispersion can vary with several orders of magnitudes from  
 247 element to element. For such a situation, the edge concentration can be significantly different  
 248 from the average of the mean concentrations of adjacent elements. Furthermore, the advective  
 249 flux is not uniquely defined at the interface and can be different for the two adjacent elements  
 250  $E$  and  $E'$ . For instance, in the case of  $Q_i^E = Q > 0$ , the advective flux leaving the element  $E$  is  
 251  $\tilde{Q}_i^{a,E} = QC^E$ , whereas the flux entering the element  $E'$  is  $\tilde{Q}_i^{a,E'} = Q(2TC_i^E - C^E)$  which could  
 252 be different as  $TC_i^E$  is not necessarily the mean of  $C^E$  and  $C^{E'}$ . In this situation, because of  
 253 the discontinuity of the advective flux, the dispersive flux will not be continuous at the  
 254 interface since the continuity is prescribed only for the total flux.

### 255 **3.2 The lumped hybrid-MFE scheme for dispersion transport**

256 In this section, we recall the main principles of the lumped hybrid-MFE method of Younes *et*  
 257 *al.* (2006), developed to improve the stability of the MFE solution in the case of dispersive  
 258 transport.

259 Considering only dispersion, Eq. (5) simplifies to:

$$260 \quad \theta \frac{\partial C}{\partial t} + \nabla \cdot \tilde{\mathbf{q}}_d = 0 \quad (23)$$

261 As detailed above, the hybrid MFE method for Eq. (23) is based on two stages:

- 262 • *Stage1: discretization of the transient mass conservation equation over the element E:*

263 The integration of the mass conservation Eq. (23) over the element  $E$  gives (see Eq.  
264 13):

$$265 \quad \theta_E |E| \frac{\partial C_E}{\partial t} + \sum_i \tilde{Q}_i^{d,E} = 0 \quad (24)$$

- 266 • *Stage2: imposing the continuity of the flux across the edge  $i$  sharing the two elements*  
267  *$E$  and  $E'$ :*

$$268 \quad \tilde{Q}_i^{d,E} + \tilde{Q}_i^{d,E'} = 0 \quad (25)$$

269 Note that the continuity equation (25) can be interpreted as a steady state mass conservation  
270 equation at the edge level. Hence, the hybrid MFE discretization uses the transient mass  
271 conservation equation at the element level, given by Eq. (24), and the steady state mass  
272 conservation at the edge level, given by Eq. (25). With the lumped hybrid MFE method of  
273 Younes *et al.* (2006), the transient term is taken into account at the edge level. Hence, the  
274 lumped formulation uses a steady state mass conservation equation at the element level and a  
275 transient mass conservation equation at the edge level. The two stages of the lumped hybrid  
276 MFE are as follows:

- 277 • *Stage1: discretization of the steady-state mass conservation equation over E:*

278 The steady-state transport over the element  $E$  writes:

$$279 \quad \sum_i \tilde{Q}_i^{d,E} = 0 \quad (26)$$

280 where  $\tilde{Q}_i^{d,E}$  is the steady-state dispersive flux across the edge  $E_i$ .

281 Therefore, the mean concentration of Eq. (15) becomes

282 
$$C_E = \sum_i \frac{\tilde{\alpha}_i^E}{\tilde{\alpha}^E} TC_i^E \quad (27)$$

283 and using Eq. (16), the steady-state dispersive flux writes

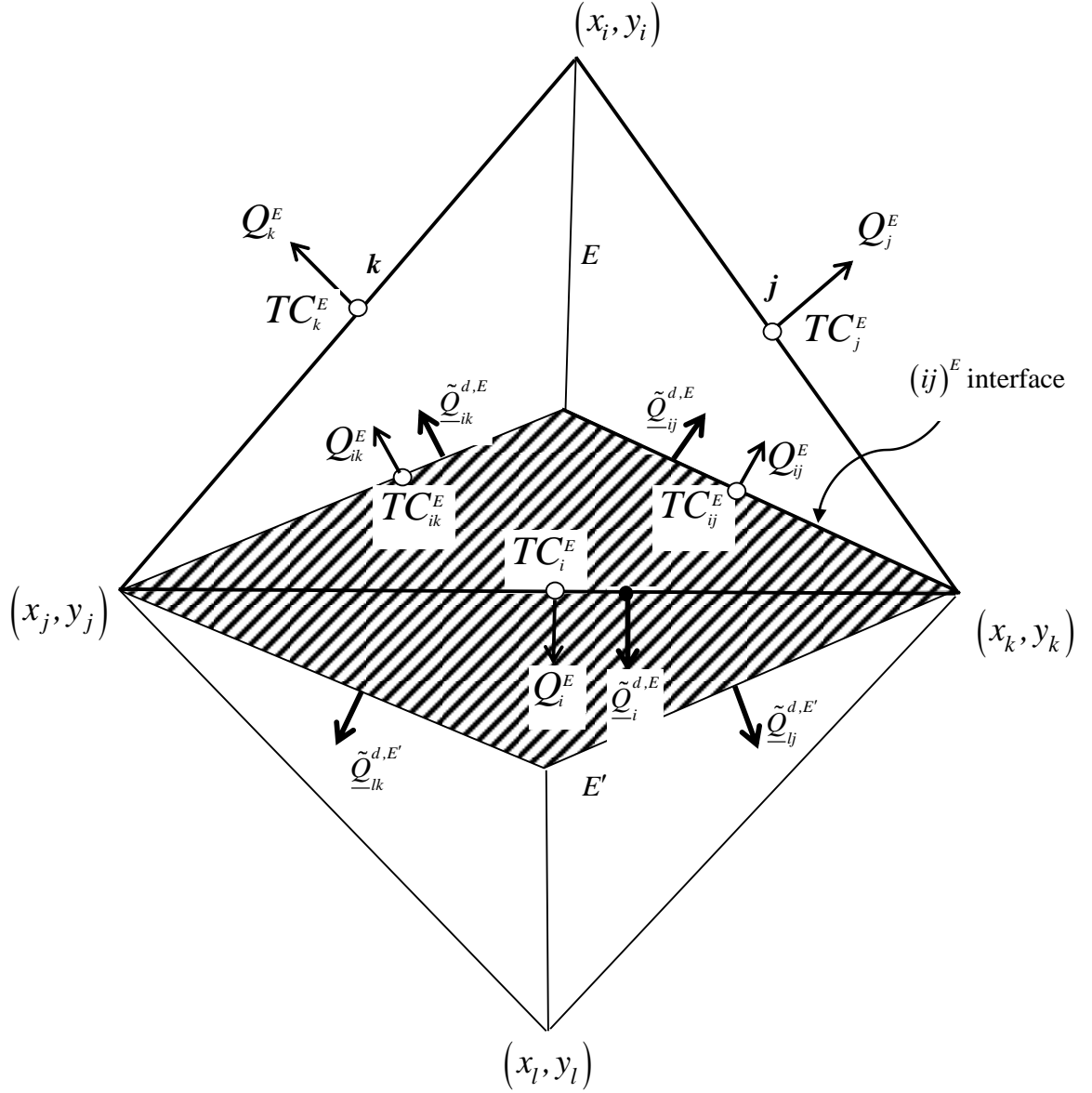
284 
$$\tilde{Q}_i^{d,E} = \sum_j \left( \frac{\tilde{\alpha}_i^E \tilde{\alpha}_j^E}{\tilde{\alpha}^E} - \tilde{B}_{i,j}^{E,-1} \right) TC_j^E \quad (28)$$

- 285 • *Stage2: discretization of the transient mass conservation equation over the lumping*  
 286 *region  $R_i$*

287 The edge centered finite volume discretization of the transient transport Eq. (23) over  
 288 the lumping region  $R_i$  (hatched area in Figure 3), associated with the edge  $i$ , writes:

289 
$$\int_{R_i} \theta \frac{\partial C}{\partial t} + \int_{R_i} \nabla \cdot \tilde{\mathbf{q}}_d = 0 \quad (29)$$

290 where the lumping regions  $R_i$  is formed by the two simplex regions  $S_i^E$  and  $S_i^{E'}$ , for  
 291 an inner edge  $i$  sharing the two elements  $E$  and  $E'$ , and by the sole simplex region  
 292  $S_i^E$  for a boundary edge. The simplex region  $S_i^E$  is defined by joining the centre of  $E$   
 293 with the nodes  $j$  and  $k$  forming the edge  $i$ .



294

295 Figure 3: The lumping region  $R_i$  associated with the edge  $i$ , sharing the elements  $E$  and

296  $E'$  and formed by the two simplex regions  $S_i^E$  and  $S_i^{E'}$ .

297 Associating the edge concentration  $TC_i^E$  to  $R_i$  (see Figure 3 for notations), Eq. (29) gives

298 
$$\left\{ \frac{|E|}{3} \theta_E \frac{\partial TC_i^E}{\partial t} + \tilde{Q}_{ij}^{d,E} + \tilde{Q}_{ik}^{d,E} \right\} + \{ \}' = 0 \quad (30)$$

299 in which  $\tilde{Q}_{ij}^{d,E}$  and  $TC_{ij}^E$  are respectively the dispersive flux and the concentration at the

300 interior interface  $(ij)^E$  between the simplex regions  $S_i^E$  and  $S_j^E$ . The shortcut  $\{ \}'$

301 designates the same contribution as  $\{ \}$ , but of the adjacent element  $E'$ , in the case of Eq.

302 (30), it corresponds to  $\frac{|E'|}{3} \theta_{E'} \frac{\partial TC_i^E}{\partial t} + \underline{\tilde{Q}}_{ij}^{d,E'} + \underline{\tilde{Q}}_{ik}^{d,E'}$ .

303 Besides, applying the steady-state dispersive transport Eq. (26) on the simplex region  $S_i^E$   
 304 yields:

305 
$$\underline{\tilde{Q}}_{ij}^{d,E} + \underline{\tilde{Q}}_{ik}^{d,E} + \underline{\tilde{Q}}_i^{d,E} = 0 \quad (31)$$

306 Finally, substituting Eq. (28) and Eq. (31) into the transport Eq. (30) give the final system  
 307 to solve with the lumped hybrid MFE scheme:

308 
$$\left\{ \frac{|E|}{3} \theta_E \frac{\partial TC_i^E}{\partial t} + \sum_j \left( \tilde{B}_{i,j}^{E,-1} - \frac{\tilde{\alpha}_i^E \tilde{\alpha}_j^E}{\tilde{\alpha}^E} \right) TC_j^E \right\} + \{ \}' = 0 \quad (32)$$

309 Note that

- 310 1. The lumped hybrid formulation Eq. (32) and the standard hybrid formulation (Eqs (24)-  
 311 (25)) are exactly the same in the case of steady state diffusion transport.
- 312 2. In the lumped formulation Eq (32), the term of mass (with time derivative) has a  
 313 contribution only on the diagonal term of the final system matrix. This improves the  
 314 monotonous character of the solution (see Younes *et al.*, 2006). For instance, in the case  
 315 of an acute triangulation, the maximum principle is respected by the lumped  
 316 formulation Eq. (32) whatever the heterogeneity of the porous medium (Younes *et al.*,  
 317 2006).
- 318 3. Contrarily to the standard hybrid-MFE scheme, where the discretization of the temporal  
 319 derivative performed in Eq. (14) was necessary to obtain the final system given by Eq.  
 320 (18), the lumped scheme given by Eq. (32) keeps the time derivative continuous which  
 321 allows the use of efficient high order temporal discretization methods via the MOL.
- 322 4. In the case of 2D triangular elements, the lumped formulation Eq. (32) is algebraically  
 323 equivalent to the nonconforming Crouzeix-Raviart (Crouzeix and Raviart, 1973) finite



324 element method (see Younes *et al.*, 2008). The nonconforming Crouzeix-Raviart  
 325 method uses the chapeau functions as basis functions to approximate the concentration,  
 326 like the standard finite element method, but seed nodes are the midpoints of the edges.

#### 327 **4. The new upwind-hybrid MFE scheme for advection-dispersion transport**

328 To avoid the rough approximation (21), we develop hereafter a new upwind-MFE scheme  
 329 where the advection term is calculated using upwind edge concentration instead of upwind  
 330 mean concentration of the element  $E$ . The idea of the scheme is to extend the lumped hybrid-  
 331 MFE procedure to transport by both advection and dispersion and to use an upwind edge  
 332 centered FV scheme to avoid unphysical oscillations caused by the hyperbolic nature of  
 333 advection.

334 The integration of the whole mass conservation Eq. (5) over the lumping region  $R_i$  writes:

$$335 \quad \int_{R_i} \theta \frac{\partial C}{\partial t} + \int_{R_i} \nabla \cdot (\mathbf{q}C) + \int_{R_i} \nabla \cdot \tilde{\mathbf{q}}_d - \int_{R_i} C \nabla \cdot \mathbf{q} = 0 \quad (33)$$

336 Using notations of Figure 3, we obtain

$$337 \quad \left\{ \frac{|E|}{3} \theta_E \frac{\partial TC_i^E}{\partial t} + Q_{ij}^E TC_{ij}^E + Q_{ik}^E TC_{ik}^E + \tilde{Q}_{ij}^{d,E} + \tilde{Q}_{ik}^{d,E} - TC_i^E (Q_{ij}^E + Q_{ik}^E) \right\} + \{ \}' = 0 \quad (34)$$

338 in which  $Q_{ij}^E$  is the water flux at the interior interface  $(ij)^E$ , evaluated using the RT0  
 339 approximation of the velocity given by Eq. (6), which yields

$$340 \quad Q_{ij}^E = \frac{1}{3} (Q_j^E - Q_i^E) \quad (35)$$

341 Using Eq (28) and Eq. (31) and denoting  $\lambda_E = \theta_E \frac{|E|}{3}$ , Eq. (34) becomes

$$342 \quad \left\{ \lambda_E \frac{\partial TC_i^E}{\partial t} + \sum_j \left( \tilde{B}_{i,j}^{E,-1} - \frac{\tilde{\alpha}_i^E \tilde{\alpha}_j^E}{\tilde{\alpha}^E} \right) TC_j^E + Q_{ij}^E TC_{ij}^E + Q_{ik}^E TC_{ik}^E - (Q_{ij}^E + Q_{ik}^E) TC_i^E \right\} + \{ \}' = 0 \quad (36)$$

343 The interior concentration  $TC_{ij}^E$  at the interface between the simplex regions  $S_i^E$  and  $S_j^E$  is  
 344 calculated using an upwind scheme (See Figure 3) defined by:

$$345 \quad TC_{ij}^E = \tau_{ij}^E TC_i^E + (1 - \tau_{ij}^E) TC_j^E \quad (36)$$

346 with  $\tau_{ij}^E = 1$  if  $(Q_{ij}^E \geq 0)$ , else  $\tau_{ij}^E = 0$

347 Thus, the final system to solve becomes,

$$348 \quad \left\{ \lambda_E \frac{\partial TC_i^E}{\partial t} + \sum_j \left( \tilde{B}_{i,j}^{E,-1} - \frac{\tilde{\alpha}_i^E \tilde{\alpha}_j^E}{\tilde{\alpha}^E} \right) TC_j^E + Q_{ij}^E (1 - \tau_{ij}^E) (TC_j^E - TC_i^E) + Q_{ik}^E (1 - \tau_{ik}^E) (TC_k^E - TC_i^E) \right\} \\ + \{ \}' = 0$$

349 (37)

350 In the case of a first-order Euler implicit time discretization, Eq. (37) becomes

$$351 \quad \left\{ \sum_j \left( \tilde{B}_{i,j}^{E,-1} - \frac{\tilde{\alpha}_i^E \tilde{\alpha}_j^E}{\tilde{\alpha}^E} \right) TC_j^{E,n+1} + \lambda_E TC_i^{E,n+1} + Q_{ij}^E (1 - \tau_{ij}^E) (TC_j^{E,n+1} - TC_i^{E,n+1}) \right\} + \{ \}' = 0 \quad (38) \\ \left\{ + Q_{ik}^E (1 - \tau_{ik}^E) (TC_k^{E,n+1} - TC_i^{E,n+1}) - \lambda_E TC_i^{E,n} \right\}$$

352 where  $\lambda_E = \theta_E \frac{|E|}{3\Delta t}$ .

353 It is easy to see that, due to upwinding, the system matrix corresponding to Eq. (38) is always  
 354 an  $M$ -matrix (a non singular matrix with  $m_{ii} > 0$ ,  $m_{ij} \leq 0$ ) in the case of transport by advection.

355 The  $M$ -matrix property insures the stability of the scheme since it guaranties the respect of the  
 356 discrete maximum principle *i.e.* local maxima or minima will not appear in the  $C$  solution in  
 357 a domain without local sources or sinks.

358 Further, Eq. (37) expresses the total exchange between  $E$  and  $E'$  and therefore reflects the  
 359 continuity of the total advection-dispersion flux between them. Both advective and dispersive  
 360 fluxes are continuous between the adjacent elements  $E$  and  $E'$ . The advective flux, calculated  
 361 using the upwind edge concentration, is uniquely defined at the interface of the lumping  
 362 region and is therefore continuous. As a consequence, the dispersive flux is also continuous

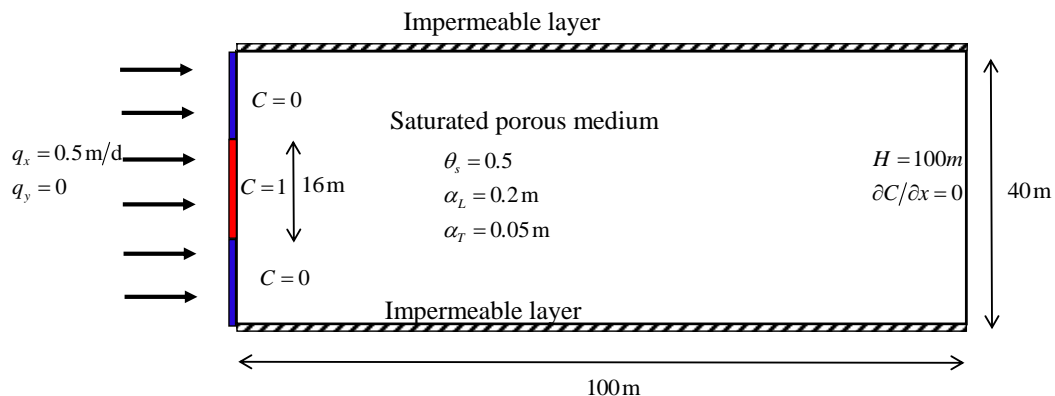
363 between  $E$  and  $E'$  since the total flux is continuous at the interface between them.

## 364 5. Numerical Experiments

365 In this section, a first test case dealing with transport in saturated porous media is simulated  
 366 with the standard hybrid-MFE and the new upwind-MFE schemes. The results are compared  
 367 against an analytical solution in order to validate the new developed scheme and to show its  
 368 robustness for solving advection-dominated transport problems compared to the standard one.  
 369 The second test case deals with transport in the unsaturated zone and aims to investigate the  
 370 robustness of the new scheme when combined with the MOL for solving highly nonlinear  
 371 problems.

### 372 5.1 Transport in saturated porous media: comparison against a 2D analytical solution

373 The hybrid and upwind MFE formulations are compared against the analytical solution  
 374 developed by Leij and Dane (1990) for a simplified 2D transport problem (Figure 4). The test  
 375 case has been employed by Putti *et al.* (1990) and Siegel *et al.* (1997) for the verification of  
 376 transport codes. It deals with the contamination from the left boundary of a 2D rectangular  
 377 domain of dimension  $(0,100) \times (0,40)$ .



378  
 379 Figure 4: Description of the problem of the contamination of a 2D saturated porous medium.

380 The boundary conditions for the transport are of Dirichlet type at the inflow (left vertical  
 381 boundary), with

$$C = \begin{cases} 0 & \text{for } x=0 \text{ and } 0 \leq y < 12 \\ 1 & \text{for } x=0 \text{ and } 12 \leq y \leq 28 \\ 0 & \text{for } x=0 \text{ and } 28 < y \leq 40 \end{cases} \quad (39)$$

383 A zero diffusive flux is imposed at the right vertical outflow boundary. The top and bottom  
384 are impermeable boundaries. A uniform horizontal flow occurs from left to right with a  
385 constant flux  $q_x = 0.5$  m/day prescribed at the left vertical boundary and a fixed head  
386  $H = 100$  m at the right vertical boundary. The longitudinal and transverse dispersivities are  
387  $\alpha_L = 0.2m$  and  $\alpha_T = 0.05m$ , respectively. The domain is discretized with a fine unstructured  
388 triangular mesh formed by 33216 elements, and the simulation is performed for a final  
389 simulation time  $T = 30$  days using the Euler-implicit time discretization with a fixed time step  
390 of 0.1 day. The linear systems are solved in each time step with a direct solver using an  
391 unsymmetric-pattern multifrontal method and a direct sparse LU factorization (UMFPACK).  
392 The analytical solution of this test case for an infinite domain is given by Leij and Dane  
393 (1990):

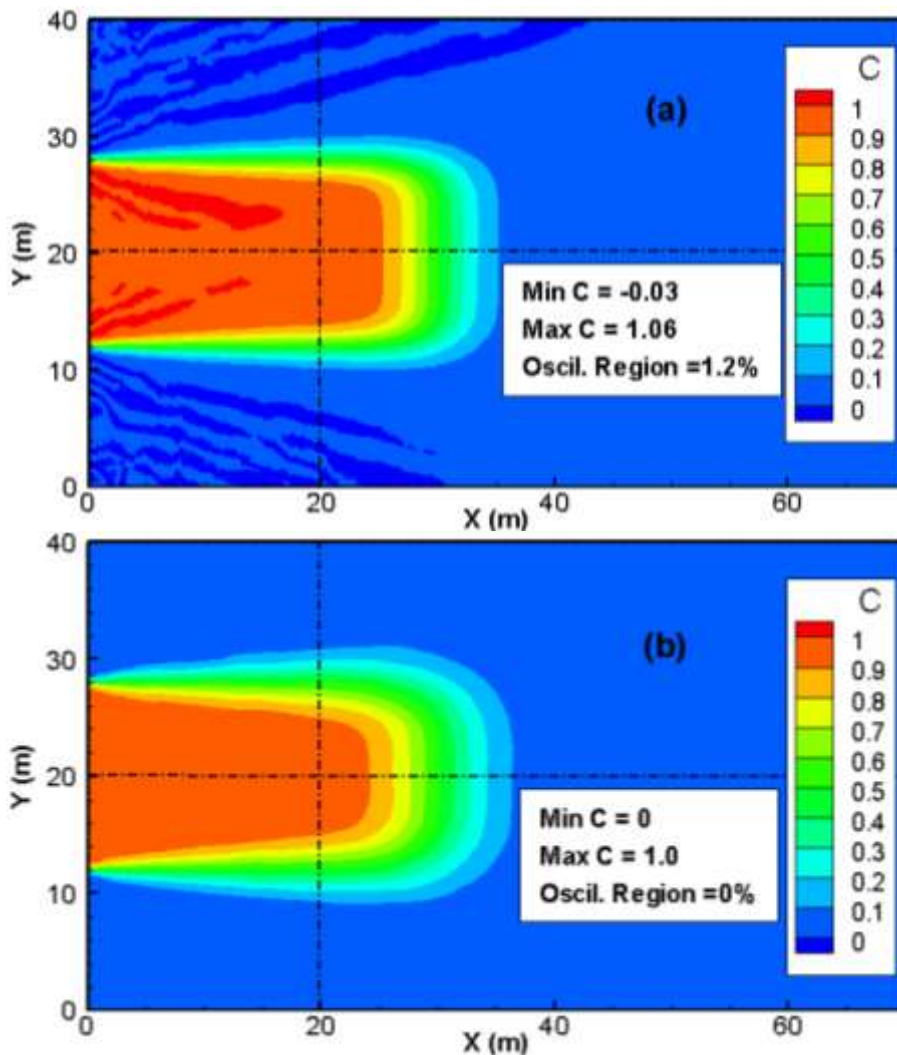
$$C_{analy}(x, y, t) = \frac{x}{(16\pi\alpha_L)^{1/2}} \int_0^T \tau^{-3/2} \left\{ \operatorname{erf} \left[ \frac{y-12}{(4\alpha_T\tau)^{1/2}} \right] + \operatorname{erf} \left[ \frac{28-y}{(4\alpha_T\tau)^{1/2}} \right] \right\} \exp \left[ -\frac{(x-\tau)^2}{4\alpha_L\tau} \right] d\tau \quad (40)$$

$$\text{with } \operatorname{erf}(x) = \frac{2}{\sqrt{\pi}} \int_0^x \exp(-\tau^2) d\tau .$$

397 The final distributions of the concentration with both hybrid-MFE and upwind-MFE schemes  
398 are depicted in Figure 5. Although we have used an unstructured mesh, the two schemes yield  
399 almost symmetrical results. The hybrid-MFE scheme (Figure 5a) yields a solution with  
400 unphysical oscillations. Indeed, around 1.2 % of the contaminated region (*i.e.* the region with  
401  $|C| \geq 10^{-5}$ ) exhibits unphysical oscillations with 0.4 % of the contaminated region with  
402  $C \leq -10^{-3}$  and 0.8 % of the contaminated region with  $C \geq 1.001$ . These unphysical  
403 oscillations, although they seem moderate, can be dramatic, for instance, when dealing with

404 reactive transport where some reactions occur only if the concentration exceeds a certain  
405 threshold. The solution obtained with the new upwind formulation (Figure 5b) is monotone  
406 (all concentrations are between 0 and 1) which is in agreement with the physics. However,  
407 these results come at the expense of some numerical diffusion added to the solution. To  
408 appreciate the quality of both solutions and validate the upwind-MFE method, we compare  
409 the concentration profile of the two methods to the analytical solution of Leij and Dane (1990)  
410 for a horizontal section located at  $y = 20$  m and a vertical section located at  $x = 20$  m.

411



412

413

414

Figure 5: Concentration distribution with the hybrid-MFE and the upwind-MFE methods for

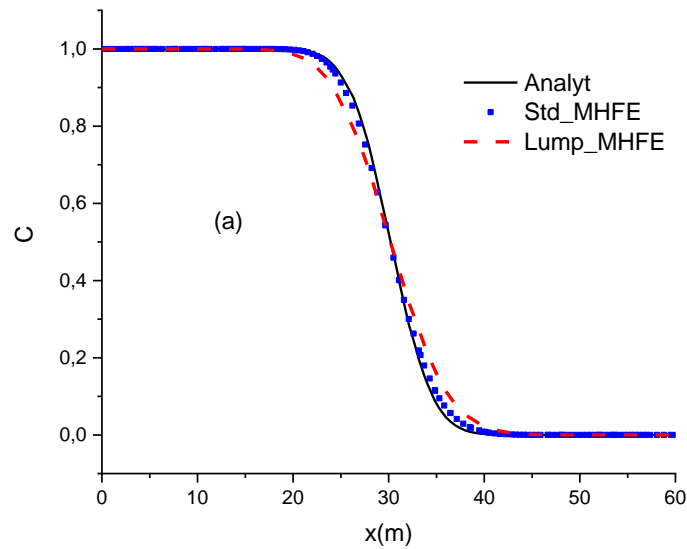
415

the 2D saturated transport problem (only the region  $x \leq 70$  m is depicted).

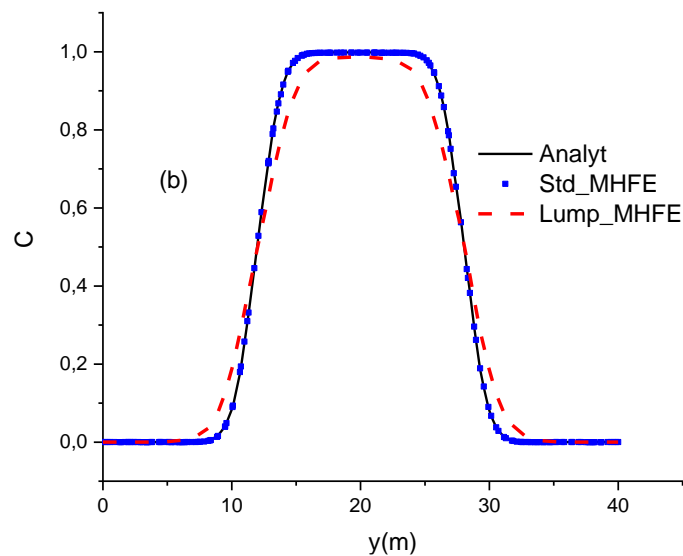
416

417 The results of figure 6 show that the solution of both hybrid-MFE and upwind-MFE methods  
418 are in very good agreement with the analytical solution, which validates the new upwind-  
419 MFE numerical model. Note, however, that a small numerical diffusion is observed with the  
420 upwind-MFE solution, which is especially visible in figure 6b. Indeed, for the simulated  
421 problem, the transverse dispersivity is much smaller than the longitudinal one, and, as a  
422 consequence, the concentration front is sharper in the vertical section than in the horizontal  
423 one. This explains why the numerical diffusion generated by the upwind-MFE method is  
424 more pronounced in Figure 6b than in Figure 6a.

425



426



427

428 Figure 6: Concentration profiles at  $y = 20\text{m}$  (a) and  $x = 20\text{m}$  (b) with the analytical, hybrid-  
 429 MFE and upwind-MFE solutions.

430 The test problem is then simulated using different mesh refinements to investigate the order of  
 431 convergence of the new method. We start with a uniform mesh formed by 1000 triangles and  
 432 a time step  $\Delta t = 0.1\text{s}$ . In each level of refinement, each triangle is subdivided into four similar  
 433 triangles, by joining the three mid-edges and the time step  $\Delta t$  is halved. The following error  
 434 is computed (Brunner *et al.*, 2014):

$$435 \quad Er = \left\{ \left\| C_{analyt}(t^N) - C(t^N) \right\|_0^2 + \Delta t \sum_{n=1}^N \left\| \tilde{\mathbf{q}}_{analyt}^t(t^n) - \tilde{\mathbf{q}}^t(t^n) \right\|_0^2 \right\}^{1/2} \quad (39)$$

436 where  $\tilde{\mathbf{q}}^t = \tilde{\mathbf{q}}_a + \tilde{\mathbf{q}}_d$  is the total advection-dispersion flux and  $N$  the total number of time  
 437 steps.

438 The runs are performed on a single computer with an Intel Xeon E-2246G processor and 32  
 439 GB memory. The results of the computations, summarized in Table 1, clearly show optimal  
 440 first order convergence in space and time for the developed upwind-hybrid MFE method.

Ref. level	# unknowns	Error $Er$	Reduction	CPU time (s)
1	1535	2.55		4.9
2	6070	1.296	1.97	38.6
3	24140	0.655	1.98	272
4	96280	0.329	1.99	2068
5	384560	0.165	2.00	16567

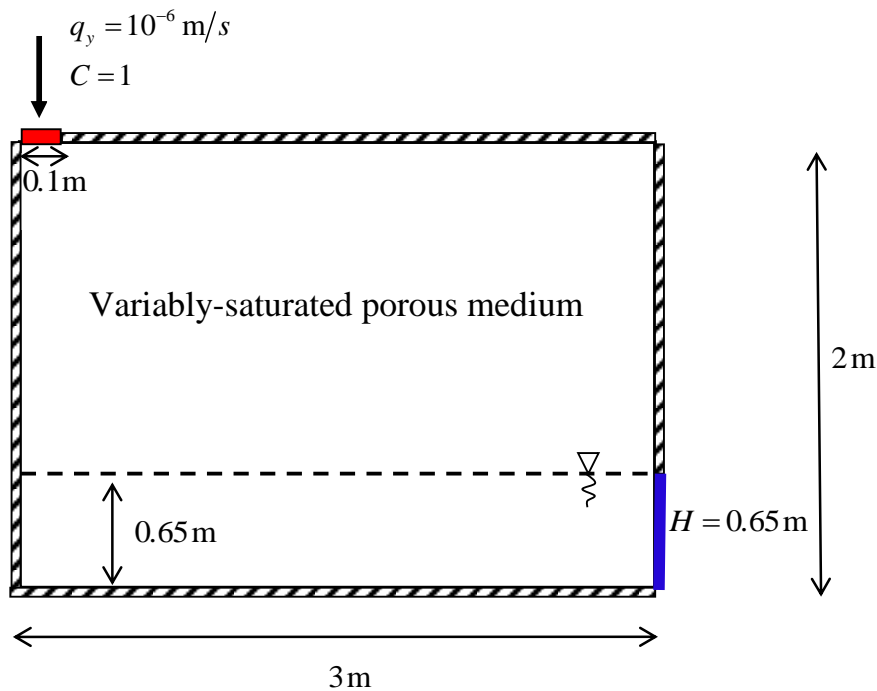
441 Table 1: Numerical results for the new upwind-hybrid MFE method.

## 442 5.2 Transport in a variably-saturated porous medium

443 In this test case, the developed upwind-MFE method is combined with the MOL for solving  
 444 contaminant transport in a variably-saturated porous medium. The advection-dispersion  
 445 equation is transformed to an Ordinary Differential Equation (ODE) using the new upwind-

446 MFE formulation for the spatial discretization, whereas the time derivative is maintained  
 447 continuous. Therefore, high-order time integration methods included in efficient ODE solvers  
 448 can be employed. With these solvers, both the time step size and the order of the time  
 449 integration can vary during the simulation to deliver accurate results in an acceptable  
 450 computational time.

451 To investigate the robustness and efficiency of the combination of the developed upwind-  
 452 MFE method with the MOL, we simulate in this section the problem of contaminant  
 453 infiltration into a variably-saturated porous medium.



454 3m  
 455 Figure 7: Description of the problem of contaminant infiltration into a 2D variably-saturated  
 456 porous medium.

457  
 458 The domain (Figure 7) is a rectangular box of  $3\text{m} \times 2\text{m}$ , filled with sand, with an initial water  
 459 table at 0.65m and hydrostatic pressure distribution. An infiltration of a tracer contaminant is  
 460 applied over the left-most 0.1m of the surface with a constant flux of  $10^{-6} \text{ m/s}$ . The right  
 461 vertical side has a fixed head  $H = 0.65 \text{ m}$  below the water table and an impermeable boundary



462 above it. The left vertical side as well as the upper (except the infiltration zone) and bottom  
 463 boundaries are impermeable boundaries.

464 In this problem, the flow and transport are coupled by the velocity, which is obtained by  
 465 solving the following pressure-head form of the nonlinear Richards' equation:

$$466 \quad \left( c(h) + S_s \frac{\theta}{\theta_s} \right) \frac{\partial H}{\partial t} + \nabla \cdot \mathbf{q} = 0 \quad (40)$$

$$467 \quad \mathbf{q} = -k_r \mathbf{K} \nabla H \quad (41)$$

468 with  $S_s$  the specific mass storativity related to head changes [ $L^{-1}$ ],  $H = h + y$  the equivalent

469 head [ $L$ ],  $h = \frac{P}{\rho g}$  the pressure head,  $P$  the pressure [ $\text{Pa}$ ],  $\rho$  the fluid density [ $\text{ML}^{-3}$ ],  $g$  the

470 gravity acceleration [ $\text{LT}^{-2}$ ],  $y$  the upward vertical coordinate [ $L$ ],  $c(h)$  the specific moisture

471 capacity [ $L^{-1}$ ],  $\theta_s$  the saturated water content [ $L^3 L^{-3}$ ],  $\mathbf{q}$  the Darcy velocity [ $\text{LT}^{-1}$ ],

472  $\mathbf{K} = \frac{\rho g}{\mu} \mathbf{k}$  the hydraulic conductivity [ $\text{LT}^{-1}$ ],  $\mathbf{k}$  the permeability [ $L^2$ ],  $\mu$  the fluid dynamic

473 viscosity [ $\text{ML}^{-1}\text{T}^{-1}$ ] and  $k_r$  the relative conductivity [-].

474 We use the standard van Genuchten (1980) model for the relationship between water content  
 475 and pressure head:

$$476 \quad S_e = \frac{\theta(h) - \theta_r}{\theta_s - \theta_r} = \begin{cases} \frac{1}{\left(1 + |\alpha h|^n\right)^m} & h < 0 \\ 1 & h \geq 0 \end{cases} \quad (42)$$

477 where  $\alpha$  [ $L^{-1}$ ] and  $n$  [-] are the van Genuchten parameters,  $m = 1 - 1/n$ ,  $S_e$  [-] is the effective

478 saturation and  $\theta_r$  [-] is the residual water content. The conductivity-saturation relationship is

479 derived from the Mualem (1976) model:

$$480 \quad k_r = S_e^{1/2} \left[ 1 - \left( 1 - S_e^{1/m} \right)^m \right]^2 \quad (43)$$

481 The material properties of the test problem are given in Table 2.

Parameters	
$\theta_r$	0.01
$\theta_s$	0.3
$\alpha$ (cm <sup>-1</sup> )	0.033
$n$	4.1
$K$ (cm/s)	10 <sup>-2</sup>
$S_s$ (cm <sup>-1</sup> )	10 <sup>-10</sup>
$D_m$ (m <sup>2</sup> /s)	10 <sup>-9</sup>
$\rho$ (kg/m <sup>3</sup> )	1000
$\mu$ (kg/m/s)	0.001

482

483 Table 2: Parameters for the problem of infiltration into a 2D variably-saturated porous  
484 medium.

485

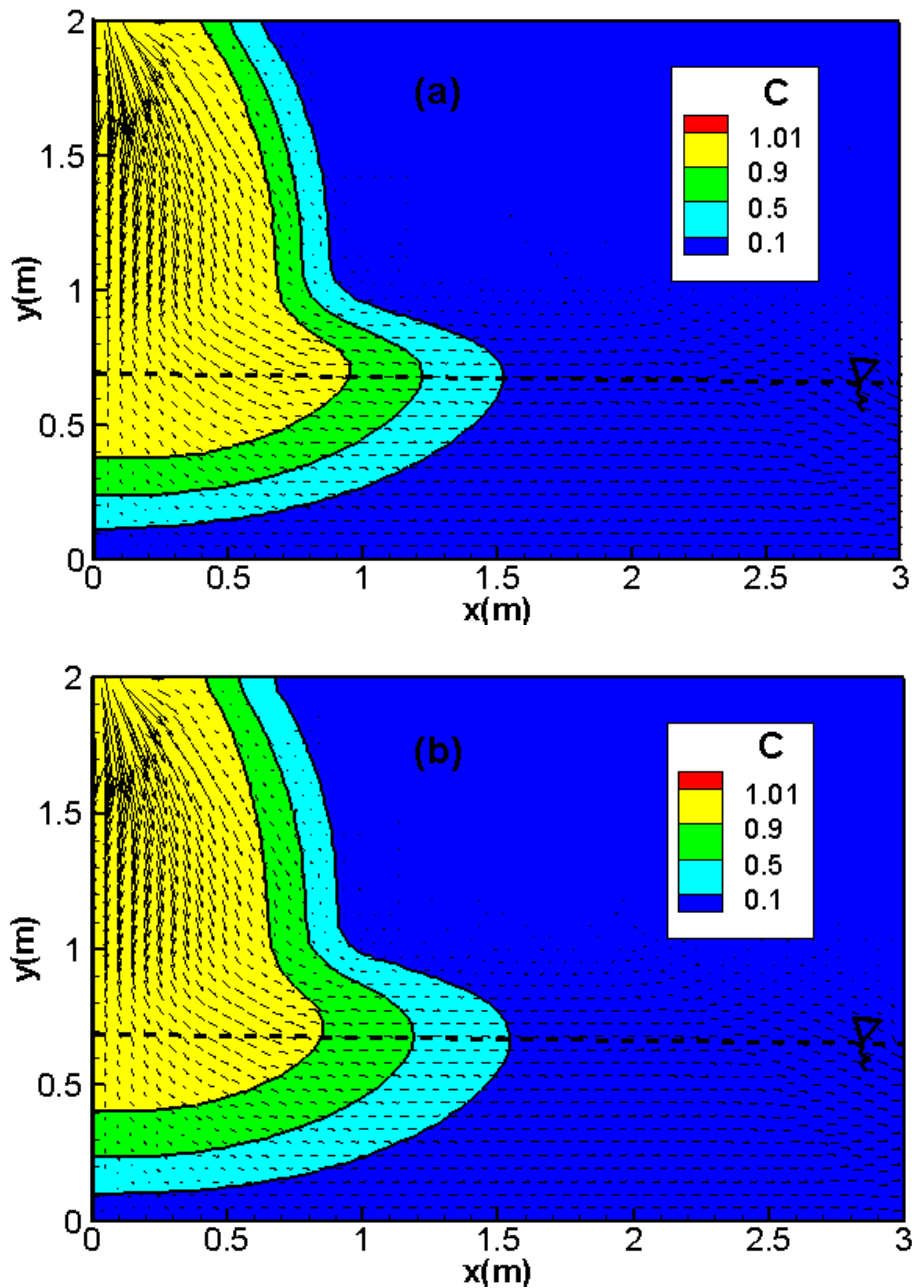
486 The simulation is performed for 80 hours using a triangular mesh formed by 4273 triangular  
487 elements. Two test cases are investigated. In the first test case, the longitudinal and transverse  
488 dispersivities are  $\alpha_L = 0.03m$  and  $\alpha_T = 0.003m$ , respectively. The second test case is less  
489 diffusive with  $\alpha_L = 0.01m$  and  $\alpha_T = 0.001m$ .

490 The coupled nonlinear flow-transport system is solved using the MOL, which allows the use  
491 of efficient high-order time integration methods, for both the hybrid-MFE and the upwind-  
492 MFE schemes. To this aim, a hybrid-MFE formulation with continuous time derivative was  
493 developed by extending the lumping procedure, developed in Younes *et al.* (2006) for the  
494 flow equation, to the advection-dispersion transport Eq. (5).

495 The time integration is performed with the DASPK time solver which uses an efficient  
496 automatic time-stepping scheme based on the Fixed Leading Coefficient Backward  
497 Difference Formulas (FLCBDF). The linear systems arising at each time step are solved with  
498 the preconditioned Krylov iterative method. The nonlinear problem is linearized using the  
499 Newton method with a numerical approximation of the Jacobian matrix.

500 The results of the hybrid-MFE and the upwind-MFE methods are depicted in Figure 8 for the

501 first test case involving high dispersion. Good agreement can be observed between the results  
502 of the hybrid-MFE (Figure 8a) and upwind-MFE (Figure 8b) schemes when combined with  
503 the MOL. In these figures, the contaminant progresses essentially vertically through the  
504 unsaturated zone of the soil. When the saturated zone is reached, the contaminant progresses  
505 horizontally and remains close to the water table. Note that the results of both schemes are  
506 stable and free from unphysical oscillations (Figures 8a and 8b).



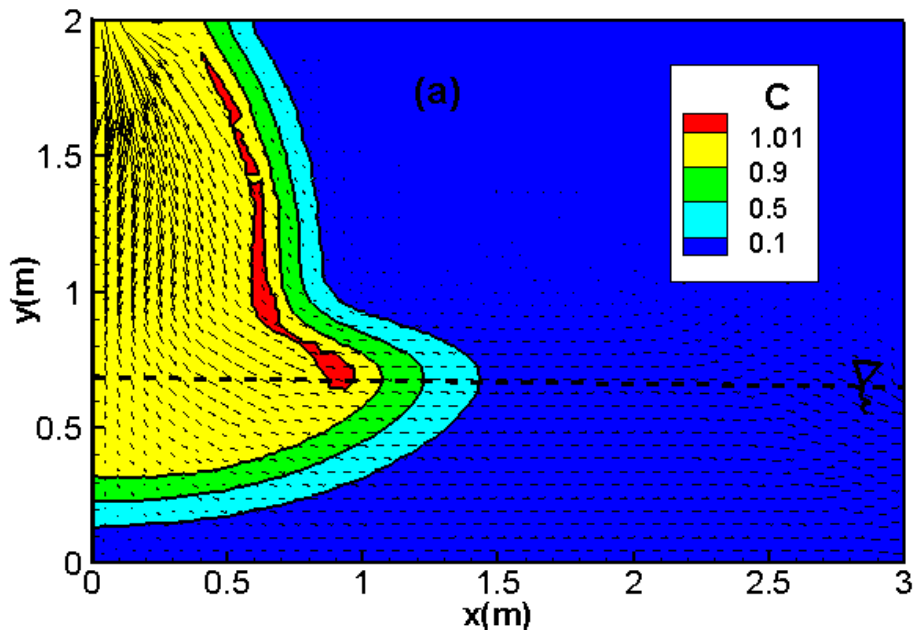
508

509

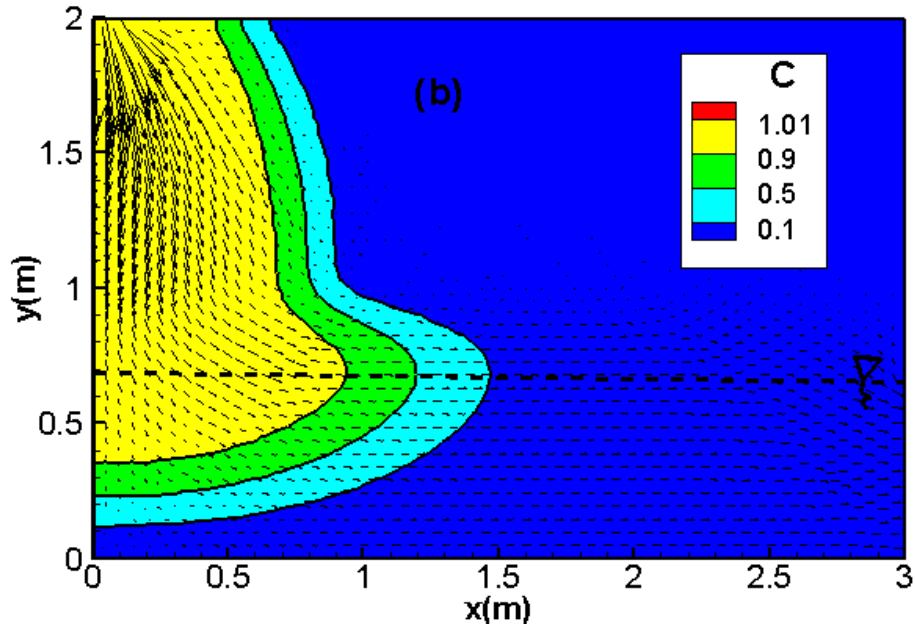
Figure 8: Concentration distribution, with the hybrid-MFE (a) and the upwind-MFE (b)

510 schemes for the transport problem with high dispersion in a variably-saturated porous  
511 medium.

512 For the second test case with lower dispersion ( $\alpha_L = 0.01m$ ,  $\alpha_T = 0.001m$ ), the hybrid-MFE  
513 method yields unstable results containing unphysical oscillations (red color in Figure 9a).  
514 These oscillations hamper the convergence of the numerical model, and severe convergence  
515 issues can be encountered if we further decrease the dispersivity values. The results of the  
516 upwind-MFE scheme are monotone and do not contain any unphysical oscillation (Figure 9b).  
517 These results point out the robustness of the new upwind MFE method for transport in  
518 saturated and unsaturated porous media. The developed transport scheme has recently been  
519 successfully combined with the MFE method for fluid flow to simulate nonlinear flow and  
520 transport in unsaturated fractured porous media using the 1D-2D discrete fracture matrix  
521 (DFM) approach (Younes et al., 2022b).



522



523

524 Figure 9: Concentration distribution with the hybrid-MFE (a) and upwind-MFE (b) methods  
 525 for the transport problem with low dispersion in variably-saturated porous medium.

## 526 6. Conclusion

527

528 MFE is a robust numerical method well adapted for diffusion problems on heterogeneous  
 529 domains and unstructured meshes. When applied to transport equations, the MFE solution can  
 530 exhibit strong unphysical oscillations due to the hyperbolic nature of advection. Upwind  
 531 schemes can be used to avoid such oscillations, although they introduce some numerical  
 532 diffusion. In this work, we developed an upwind scheme that does not require any  
 533 approximation for the upwind concentration. The method can be seen as a combination of an  
 534 upwind edge/face centred FV method with the lumped formulation of the hybrid-MFE  
 535 method. It ensures continuity of both advective and dispersive fluxes between adjacent  
 536 elements and allows to maintain the time derivative continuous, which facilitates employment  
 537 of high order time integration methods via the method of lines (MOL) for nonlinear problems.  
 538 Numerical simulations for the transport in a saturated porous medium show that the standard  
 539 hybrid-MFE method can generate unphysical oscillations due to the hyperbolic nature of

540 advection. These unphysical oscillations are completely avoided with the new upwind-MFE  
541 scheme. The simulation of the problem of contaminant transport in a variably-saturated  
542 porous medium shows that only the upwind-MFE scheme provides a stable solution. The  
543 results point out the robustness of the developed upwind-MFE scheme when combined with  
544 the MOL for solving nonlinear transport problems.

545

546

547

548

## References

- 550 Belfort, B., Ramasomanana, F., Younes, A., and Lehmann, F.: An Efficient Lumped Mixed  
551 Hybrid Finite Element Formulation for Variably Saturated Groundwater Flow, 8, 352–  
552 362, <https://doi.org/10.2136/vzj2008.0108>, 2009.
- 553 Brezzi, F. and Fortin, M. (Eds.): Mixed and Hybrid Finite Element Methods, Springer New  
554 York, New York, NY, <https://doi.org/10.1007/978-1-4612-3172-1>, 1991.
- 555 Brezzi, F., Douglas, J., and Marini, L. D.: Two families of mixed finite elements for second  
556 order elliptic problems, *Numer. Math.*, 47, 217–235,  
557 <https://doi.org/10.1007/BF01389710>, 1985.
- 558 Brunner, F., Radu, F. A., and Knabner, P.: Analysis of an Upwind-Mixed Hybrid Finite  
559 Element Method for Transport Problems, *SIAM J. Numer. Anal.*, 52, 83–102,  
560 <https://doi.org/10.1137/130908191>, 2014.
- 561 Chavent, G. and Jaffré, J.: Mathematical models and finite elements for reservoir simulation:  
562 single phase, multiphase, and multicomponent flows through porous media, North-  
563 Holland ; Sole distributors for the U.S.A. and Canada, Elsevier Science Pub. Co,  
564 Amsterdam ; New York : New York, N.Y., U.S.A, 376 pp., 1986.
- 565 Chavent, G. and Roberts, J. E.: A unified physical presentation of mixed, mixed-hybrid finite  
566 elements and standard finite difference approximations for the determination of  
567 velocities in waterflow problems, 14, 329–348, [https://doi.org/10.1016/0309-1708\(91\)90020-O](https://doi.org/10.1016/0309-1708(91)90020-O), 1991.
- 569 Crouzeix, M., Raviart, P.A. Conforming and nonconforming finite element methods for  
570 solving the stationary Stokes equations, *R.A.I.R.O. R3*, 7, 33-76, 1973.
- 571 Dawson, C.: Analysis of an Upwind-Mixed Finite Element Method for Nonlinear contaminant  
572 Transport Equations, *SIAM J. Numer. Anal.*, 35, 1709–1724,  
573 <https://doi.org/10.1137/S0036142993259421>, 1998.
- 574 Dawson, C. N. and Aizinger, V.: Upwind mixed methods for transport equations, 3, 93–110,  
575 1999.
- 576 Fahs, M., Younes, A., and Lehmann, F.: An easy and efficient combination of the Mixed  
577 Finite Element Method and the Method of Lines for the resolution of Richards’  
578 Equation, *Environmental Modelling & Software*, 24, 1122–1126,  
579 <https://doi.org/10.1016/j.envsoft.2009.02.010>, 2009.
- 580 van Genuchten, M. T.: A Closed-form Equation for Predicting the Hydraulic Conductivity of  
581 Unsaturated Soils, *Soil Science Society of America Journal*, 44, 892–898,

582 <https://doi.org/10.2136/sssaj1980.03615995004400050002x>, 1980.

583 Hoteit, H., Mosé, R., Philippe, B., Ackerer, P., and Erhel, J.: The maximum principle  
584 violations of the mixed-hybrid finite-element method applied to diffusion equations:  
585 Mixed-hybrid finite element method, 55, 1373–1390, <https://doi.org/10.1002/nme.531>,  
586 2002.

587 Hoteit, H., Erhel, J., Mosé, R., Philippe, B., and Ackerer, P.: Numerical Reliability for Mixed  
588 Methods Applied to Flow Problems in Porous Media, n.d.

589 Koohbor, B., Fahs, M., Hoteit, H., Doummar, J., Younes, A., and Belfort, B.: An advanced  
590 discrete fracture model for variably saturated flow in fractured porous media, 140,  
591 103602, <https://doi.org/10.1016/j.advwatres.2020.103602>, 2020.

592 Leij, F. J. and Dane, J. H.: Analytical solutions of the one-dimensional advection equation and  
593 two- or three-dimensional dispersion equation, 26, 1475–1482,  
594 <https://doi.org/10.1029/WR026i007p01475>, 1990.

595 Mazzia, A.: An analysis of monotonicity conditions in the mixed hybrid finite element  
596 method on unstructured triangulations, 76, 351–375,  
597 <https://doi.org/10.1002/nme.2330>, 2008.

598 Mualem, Y.: A new model for predicting the hydraulic conductivity of unsaturated porous  
599 media, *Water Resour. Res.*, 12, 513–522, <https://doi.org/10.1029/WR012i003p00513>,  
600 1976.

601 Putti, M., Yeh, W.W.-G., and Mulder, W.A.: A triangular finite volume approach with high-  
602 resolution upwind terms for the solution of groundwater transport equations, *Water*  
603 *Resources Res.*, 26, 2865-2880, <https://doi.org/10.1029/WR026i012p02865>, 1990.

604 Radu, F. A., Suciu, N., Hoffmann, J., Vogel, A., Kolditz, O., Park, C.-H., and Attinger, S.:  
605 Accuracy of numerical simulations of contaminant transport in heterogeneous  
606 aquifers: A comparative study, *Advances in Water Resources*, 34, 47–61,  
607 <https://doi.org/10.1016/j.advwatres.2010.09.012>, 2011.

608 Raviart, P. A. and Thomas, J. M.: A mixed finite element method for 2-nd order elliptic  
609 problems, in: *Mathematical Aspects of Finite Element Methods*, Berlin, Heidelberg,  
610 292–315, 1977.

611 Siegel, P., Mosé, R., Ackerer, P., and Jaffré, J.: Solution of the Advection Diffusion Equation  
612 using a combination of Discontinuous and Mixed Finite Elements, *Int. J. Numer.*  
613 *Meth. Fluids*, 24: 595-613. [https://doi.org/10.1002/\(SICI\)1097-  
614 0363\(19970330\)24:6<595::AID-FLD512>3.0.CO;2-I](https://doi.org/10.1002/(SICI)1097-0363(19970330)24:6<595::AID-FLD512>3.0.CO;2-I), 1997.

615



616 Traverso, L., Phillips, T. N., and Yang, Y.: Mixed finite element methods for groundwater  
617 flow in heterogeneous aquifers, *Computers & Fluids*, 88, 60–80,  
618 <https://doi.org/10.1016/j.compfluid.2013.08.018>, 2013a.

619 Traverso, L., Phillips, T. N., and Yang, Y.: Mixed finite element methods for groundwater  
620 flow in heterogeneous aquifers, *Computers & Fluids*, 88, 60–80,  
621 <https://doi.org/10.1016/j.compfluid.2013.08.018>, 2013b.

622 Vohralík, M.: A Posteriori Error Estimates for Lowest-Order Mixed Finite Element  
623 Discretizations of Convection-Diffusion-Reaction Equations, 45, 1570–1599,  
624 <https://doi.org/10.1137/060653184>, 2007.

625 Younes, A., Mose, R., Ackerer, P., and Chavent, G.: A New Formulation of the Mixed Finite  
626 Element Method for Solving Elliptic and Parabolic PDE with Triangular Elements,  
627 149, 148–167, <https://doi.org/10.1006/jcph.1998.6150>, 1999.

628 Younes, A., Ackerer, P., and Lehmann, F.: A new mass lumping scheme for the mixed hybrid  
629 finite element method, *International Journal for Numerical Methods in Engineering*,  
630 67, 89–107, <https://doi.org/10.1002/nme.1628>, 2006.

631 Younes, A., Fahs, M., and Ahmed, S.: Solving density driven flow problems with efficient  
632 spatial discretizations and higher-order time integration methods, *Advances in Water  
633 Resources*, 32, 340–352, <https://doi.org/10.1016/j.advwatres.2008.11.003>, 2009.

634 Younes, A., Ackerer, P., and Delay, F.: Mixed finite elements for solving 2-D diffusion-type  
635 equations, *Rev. Geophys.*, 48, RG1004, <https://doi.org/10.1029/2008RG000277>, 2010.

636 Younes, A., Koohbor, B., Belfort, B., Ackerer, P., Doummar, J., and Fahs, M.: Modeling  
637 variable-density flow in saturated-unsaturated porous media: An advanced numerical  
638 model, *Advances in Water Resources*, 159,  
639 <https://doi.org/10.1016/j.advwatres.2021.104077>, 2022a.

640 Younes, A., Hoteit H., Helmig, R., and Fahs, M.: A robust fully mixed finite element model  
641 for flow and transport in unsaturated fractured porous media, *Advances in Water  
642 Resources*, Volume 166, <https://doi.org/10.1016/j.advwatres.2022.104259>, 2022b.

643  
644